Journal of Materials Chemistry B

Advancements in Organic Fluorescent Materials: Unveiling the Potential of Peripheral Group Modification in dithienyl-diketopyrrolopyrrole derivatives for One- and Two-Photon Bioimaging

Journal:	*Journal of Materials Chemistry B*
Manuscript ID	TB-ART-10-2024-002291.R1
Article Type:	Paper
Date Submitted by the Author:	15-Nov-2024

Complete List of Authors:	Zucolotto Cocca, Leandro Henrique; Universidade Federal de Goias; Universidade de São Paulo Instituto de Física de São Carlos Pereira Valverde, João; Instituto de Física de Sâo Carlos - Universidade de São Paulo, IFSC Leite, Celisnolia; Universidade de São Paulo Instituto de Física de São Carlos Moreno, Natália; Universidade de São Paulo, Physics Institute of São Carlos Neto, Alfredo L.; CP Macedo, Andreia; Universidade Tecnologica Federal do Parana Pratavieira, Sebastião; University of Sao Paulo Institute of Physics of Sao Carlos Silva, Daniel L.; Federal University of São Carlos, Department of Natural Sciences, Mathematics and Education Rodrigues, Paula C.; Universidade Tecnologica Federal do Parana, Departamento Acadêmico de Química e Biologia (DAQBi) Zucolotto, Valtencir; University of São Paulo, Physics Institute of São Carlos Mendonça, Cleber Renato; Universidade de São Paulo, FCM De Boni, Leonardo; Universidade de São Paulo Instituto de Física de São Carlos, Física e Ciência dos Materiais

Advancements in Organic Fluorescent Materials: Unveiling the Potential of Peripheral Group Modification in dithienyl-diketopyrrolopyrrole derivatives for One- and Two-Photon Bioimaging

Leandro H. Zucolotto Cocca[a*], João V. P. Valverde[b], Celisnolia M. Leite[c], Natália S. Moreno[c], Alfredo L. Neto[d], Andreia G. Macedo[d,e], Sebastião Pratavieira[b], Daniel L. Silva[f], Paula C. Rodrigues[d,e], Valtencir Zucolotto[c], Cleber R. Mendonça[b] and Leonardo De Boni[b]

[a] Photonics Group, Institute of Physics, Federal University of Goiás, Goiânia, 74690-900, GO, Brazil.
[b] Sao Carlos Physics Institute, University of São Paulo, CP 369, 13560-970 São Carlos, SP, Brazil
[c] Nanomedicine and Nanotoxicology Group, Sao Carlos Physics Institute, University of São Paulo, 13560-970 São Carlos, SP, Brazil.
[d] Graduate Program in Chemistry, Federal University of Technology – Parana (UTFPR), CP 81531-990 Curitiba, Brazil
[e] Graduate Program in Physics and Astronomy, Federal University of Technology – Paraná (UTFPR), CP 81531-990 Curitiba, Brazil
[f] Department of Natural Sciences, Mathematics and Education, Federal University of São Carlos, Rod. Anhanguera – Km 174, 13600-970 Araras, SP, Brazil

*Author to whom correspondence should be addressed: leandro.zucolottococca@gmail.com

Abstract

The quest for novel organic fluorescent materials capable of two-photon absorption (2PA) has intensified in recent years due to their promising applications in biological imaging. Two-photon fluorescence microscopy (2PFM) offers high spatial-temporal resolution, reduced photodamage, and deeper tissue penetration compared to conventional techniques. However, the development of bright two-photon molecular markers remains a challenge, necessitating compounds with high fluorescence quantum yield and 2PA cross-section (σ^{2PA}). Strategies such as increasing π-conjugation have shown promise but are hindered by synthesis complexities and limited biocompatibility. Alternatively, incorporating electron-donating (ED) or electron-withdrawing (EW) peripheral groups in a main structure has emerged as a viable approach, leading to significant enhancements in σ^{2PA}. This study highlights the advantages and challenges of these strategies, emphasizing the importance of exploring new organic compounds and evaluating the efficacy of peripheral groups for advanced two-photon bioimaging applications.

Highlights

New materials for biological imaging probes via one- and two-photon absorption

Linear and nonlinear spectroscopy

Diketopyrrolopyrroles derivatives

Two-photon absorption characterization

Evaluation of compound feasibility for biological imaging

1 INTRODUCTION

The recent interest in novel organic fluorescent materials exhibiting two-photon absorption[1,2] may be attributed to the potential application of these materials as probes in biological systems, enabling safe and non-invasive optical imaging with high spatial-temporal resolution, both *in vivo* and *in vitro*[3,4]. The motivation for this pursuit is intricately linked to the advantageous characteristics of the two-photon absorption (2PA) process compared to the common one-photon absorption (1PA) process. These include precise spatial control, the use of infrared light, commonly found in the near-infrared I and II regions (NIR-I and NIR-II: 700-900 nm and 1000-2000 nm), which circumvents issues of light scattering in turbid media and allows for greater depth of penetration[3,5]. Additionally, two-photon fluorescence bioimaging significantly reduces background fluorescence signals from endogenous fluorescent systems, as well as photobleaching and photodamage in imaging markers and molecular structures[4].

With the proliferation of two-photon fluorescence microscopes (2PFM), this technique has become invaluable for researchers in the fields of biology and biomedicine, enabling high-resolution studies of physiological, morphological, and cellular interactions in intact tissues and living animals[4,6]. However, there are still challenges that need to be overcome for a broader adoption of 2PFM, particularly related to fluorescent markers. To visualize, characterize, and quantify biological systems, bright two-photon molecular markers are required, including dyes with high fluorescence quantum yield and 2PA cross-section (σ^{2PA})[4,7]. Regarding σ^{2PA}, several strategies have been proposed to develop more efficient 2PA compounds. One of the widely used strategies is increasing the π-conjugation of the main structure. It is well-known that increasing the number of π-electrons results in a super-linear increase in the σ^{2PA}[8]. However, this strategy has several

disadvantages due to the structure's size, such as challenging synthesis routes, little flexibility for modification, and low biocompatibility[1]. Other strategies have been developed to obtain appreciable values of σ^{2PA} in smaller molecules, including the incorporation of electron-donating (ED) or electron-withdrawing (EW) peripheral groups at the ends of the main structure[9,10]. This can form symmetrical structures of the ED-π-ED or EW-π-EW type or asymmetrical structures of the EW-π-ED type, where π is a π-conjugated structure. This procedure has been extremely advantageous, with increases of up to 20 times in the 2PA cross-section already demonstrated[1,9]. Although peripheral groups significantly improve 2PA in organic compounds, it is still unknown how they influence the emissive properties and biocompatibility of these compounds. These remain open questions that require further study. Based on this, it is still necessary to research new small organic compounds and evaluate the efficiency of peripheral groups in these new organic structures. This becomes crucial, especially considering the potential of these compounds in advanced two-photon fluorescence imaging applications.

Among various organic compounds, studies have shown a growing interest in diketopyrrolopyrroles derivatives, also known as DPPs[11–15]. This is due to their remarkable properties, such as an accessible synthesis route, easy modification by incorporating substituents, high fluorescence quantum yield, and planarity, making it an extremely privileged structure[16,17]. Due to these interesting properties, such compounds are widely present in the field of materials science in studies related to organic light-emitting devices (OLEDs)[18], dye lasers[19], solar cells[20], and field-effect transistors (OFETs)[21]. Recent studies have also been carried out exploring the excellent emissive properties of these dyes as a fluorescent sensor[22] and one-photon fluorescent probe[23], revealing the great interest in studying the 2PA process in diketopyrrolopyrroles derivatives.

With respect to the ease of synthesis, Pieczykolan and collaborators introduced a novel methodology for preparing these DPP derivatives[24]. Additionally, studies have demonstrated that polarized diketopyrrolopyrroles can exhibit charge transfer modulation[12], as well as symmetry breaking in both the ground and excited states[14]. Through these works, it is possible to observe the scientific interest in the study of molecules derived from DPP. These studies highlight the growing scientific interest in DPP-derived molecules, paving the way for the development of new synthetic routes and the exploration of their optical properties.

Considering the potential applications of DPPs as 2PA fluorescent probes, particularly for living cell fluorescent microscopy, Diketopyrrolopyrrole-based fluorophores show promising results. For example, in the study of Ftouni[25] and collaborator, it was determined that the peak values of 2PA cross section reached approximately 350-750 GM at 800 nm. Additionally, fluorescence quantum efficiencies were measured, with values ranging from 34% to 70%, depending on the specific DPP derivative.

In this Scenario, here, a wide characterization of two symmetric dithienyl-diketopyrrolopyrrole derivatives of the ED-π-ED type was carried out, exploring the influence of the thienyl moiety (an electron-rich structure acting as an extension of the π-conjugation) and the bromine atom on the linear and nonlinear properties of these compounds. Several spectroscopic measurements were performed, including one-photon absorption, fluorescence, fluorescence quantum yield, fluorescence lifetime, solvatochromism, and two-photon absorption. Furthermore, quantum chemical calculations at the theoretical level DFT and TD-DFT for a better understanding of the properties of these dyes. Finally, such compounds were incorporated into Human Dermal Fibroblasts, neonatal (HDFn) cells, where toxicity tests were conducted, as well as assessments of the feasibility of these compounds as fluorescent markers for one- and two-photon imaging.

2 EXPERIMENTAL AND COMPUTATIONAL SECTION

2.1 Compounds

The dithienyl-diketopyrrolopyrrole derivatives synthesis was previously described in Ref.[20,26] and are presented in Supplementary Information. The molecules should be designated as: **DPP2T** 2,5-dihexyl-3,6-di(thiophen-2-yl)pyrrolo[3,4-c]pyrrole-1,4(2H,5H)-dione, and **DPP2TBr** 3,6-bis(5-bromothiophen-2-yl)-2,5-dihexylpyrrolo[3,4-c]pyrrole-1,4(2H,5H)-dione.

Figure 1 shows the molecular structure of the compounds, where R represents the substituent groups. To increase effective molecular conjugation and, consequently, nonlinear optical responses, both dyes contain a thienyl group at positions C-3 and C-6. The difference between the two samples is that in **DPP2TBr** the hydrogen atom in the thienyl unit is replaced by bromine. In addition, both compounds contain a hexyl chain at positions C-2 and C-5 to improve their solubility in chloroform.

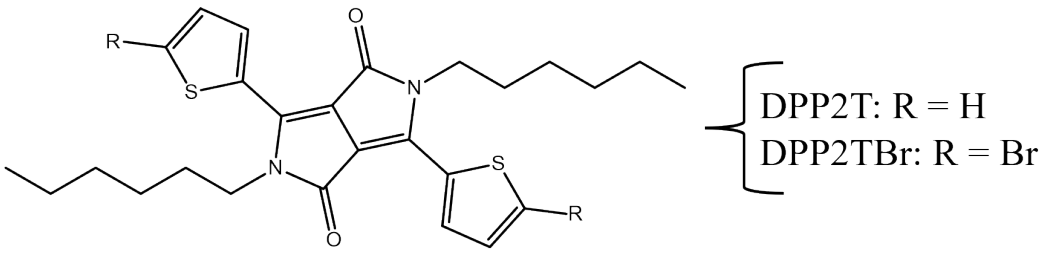

Figure 1 - Dithienyl-diketopyrrolopyrrole derivatives chemical structure.

2.2 Linear optical measurements

Dithienyl-diketopyrrolopyrrole samples were dissolved in chloroform at a concentration of *c.a.* $10^{-4}\ mol/L$ and then placed in a quartz cell with optical path length of $10\ mm$ (It should be mentioned that no effects relating to aggregation were observed). The one-photon absorption spectra were measured using a spectrophotometer (Shimadzu, model UV-1800). Steady-state emission spectra were determined by a fluorimeter (Hitachi, model F-4500). The dyes' fluorescence quantum yield (ϕ) was obtained by the well-known Brouwer method[27] using kiton-red 620 as a standard sample dissolved in ethanol ($\phi = 69\%$)[28]. The studied and standard samples fluorescence spectra were obtained under the same experimental conditions. Solvatochromism measurements were performed by dissolving the chromophores in different solvents, namely: toluene, dichloromethane (DCM), dimethylsulfoxide (DMSO), N,N-dimethylformamide (DMF), ethanol and methanol. It is noteworthy that, for measurements involving obtaining fluorescence emission, it was necessary to further dilute the solutions in the order of $10^{-6}\ mol/L$ to avoid fluorescence reabsorption[29].

The fluorescence lifetimes of the dyes were determined using the time-resolved fluorescence technique, employing a femtosecond laser system, as detailed in **Section 1** of the Supporting Information (SI). For this purpose, the samples were placed in a quartz cell with an optical path length of $2\ mm$.

2.3 Quantum chemical calculations

These Quantum chemical calculations (QCCs) based on the density functional theory (DFT) framework were conducted to aid in the interpretation of experimental results. For that, the 1PA properties (transition energy and oscillator strength) of the 20 lowest-energy singlet electronic transitions of the studied molecules were computed by time-dependent density functional theory (TD-DFT) calculations using the Gaussian 09

package[30]. The molecular orbitals related with such electronic transitions and the permanent dipole moment difference between the first excited state and ground one ($|\Delta\vec{\mu}_{01}| = |\vec{\mu}_{11} - \vec{\mu}_{00}|$, in D) were also computed. Moreover, using the quadratic response function (QRF)[31] within the DFT framework, as implemented in DALTON program[32], the 2PA transition probabilities of the five lowest-energy singlet electronic transitions of the studied molecules were computed.

Initially, geometry optimization and frequency calculations were carried out using the B3LYP[33] exchange-correlation hybrid functional with a combination of two standard basis sets: the well-known 6-311G(d,p)[34] for hydrogen, carbon, nitrogen, and oxygen atoms, and cc-pVDZ[35] for sulfur and bromine atoms. The Gaussian 09 package was used and the calculations were performed in both gas-phase and chloroform solvent. No imaginary vibrational modes were identified from the frequency calculations, indicating that fully optimized structures corresponding with stable minimum were obtained. The effects of the solvent environment on the equilibrium geometry and the spectroscopic properties of the studied molecules were taken into account by employing the polarizable continuum model (PCM). The PCM with the integral equation formalism variant (IEF-PCM)[36,37], as implemented in Gaussian 09 package, was used. The PCM was also employed to estimate the radius of the solute molecular cavity.

In the QQCs concerning the spectroscopic properties of the studied molecules, *i.e.*, the TD-DFT and QRF calculations, an approach using B3LYP functional combined with the augmented 6-311++G(d,p) (for H, C, N and O atoms) and aug-cc-pVDZ (for S and Br atoms) basis sets was used.

For the QRF calculations the PCM[38] as implemented in DALTON program was used. For the sake of consistency, for the studied molecules the van der Waals surfaces used in the QRF calculations were defined by adopting the set of van der Waals radius and atomic centers determined at the geometry optimization stage using the Gaussian 09 package. Finally, the details of the procedures for constructing the 1PA and 2PA spectra adopted here, as well as the data obtained from the calculations, can be found in **Section 2** of the SI.

2.4 Two-photon absorption measurements

Two-photon absorption measurements were performed using the well-known open-aperture tunable femtosecond Z-scan technique[39], employing a laser system (Light Conversion, Pharos-PH1 model) with a pulse duration of 220 fs centered at 1030 nm

and operating at a $750\ Hz$ repetition rate. The laser system is used to pump an optical parametric amplifier (OPA) (Light Conversion, ORPHEUS model), which allows tuning of the excitation wavelengths from $210-3000\ nm$. This enabled the σ^{2PA} determination of the compounds from $790-1000\ nm$, with a spectral resolution of $10\ nm$. Details on the technique and curve fitting procedure can be found in **Section 3** of the SI.

Measurements of fluorescence emission excited by 2PA were performed by exciting the compounds at $850\ nm$ and $900\ nm$. For this purpose, the same laser system was employed, operated at a repetition rate of $1.5\ kHz$, with different excitation powers. A more detailed description of the procedure can be found in **Section 4** of the SI.

2.5 Cell culture

The HDFn cell line (Human Dermal Fibroblast neonatal) was cultured with Dulbecco's Modified Eagle Medium (DMEM; Vitrocell® Embriolife) supplemented with 10% fetal bovine serum (FBS). The cells were incubated at 37 °C in a humidified atmosphere with 5% CO_2.

2.6 Cell toxicity.

3-[4,5-dimethyl-thiazol-2-yl]-2,5- diphenyltetrazolium bromide (MTT) colorimetric assay was employed to evaluate the cytotoxicity of **DPPT2** and **DPPT2Br** compounds. HDFn cells were initially seeded at a density of 1×10^4 cells/ well in a 96-well plate and cultured for 24 hours in 100 µL of DMEM medium supplemented with 10% FBS. Subsequently, the medium was replaced by 100 µL of fresh medium containing varying concentrations of the compounds, along with a negative control (0.5% DMSO). Following 1, 4, and 24 hours of incubation at 37°C, the medium containing the compounds was exchanged with MTT-containing medium (0.5 mg/mL) and further incubated for 1 hour. Cell viability was assessed by monitoring the reduction of MTT to purple formazan within live cells. Formazan crystals were then solubilized using DMSO (200 µL/well), and the optical density of each well was measured at a wavelength of 570 nm using a microplate reader (SpetramaxM3). The cell viability data were derived from absorbance analysis across three independent experiments.

2.7 Cellular internalization

In flow cytometric analysis, HDFn cells were seeded at a density of 1×10^5 cells/well in 12-well plates and cultured for 24 hours in 1 mL of DMEM medium containing 10% FBS. Subsequently, the compounds, DPP2T and DPP2TBr, were coincubated with the cells at a concentration of 0.5 μM for 1, 4, and 24 hours to monitor the cellular uptake of these compounds. Following coincubation, the cells were washed three times with PBS, detached by trypsin-EDTA, and collected by centrifugation at 1000 g for 10 minutes. Afterward, the cells were washed and resuspended in 400 μL of Sheath Fluid (BD Bioscience) for analysis on the flow cytometer. Data were collected using a FACSCalibur, recording 10000 events. The subsequent analysis used Flowjo software, with untreated cells as the negative control.

2.8 Cellular bioimaging

HDFn cells were seeded on glass coverslips in a 24-well plate (2.5×10^4 cells/well). After overnight incubation, the cells were treated with 0.5 μM of **DPP2T** and **DPP2TBr** for 1 hour. Subsequently, the cells were carefully washed with PBS and fixed with 4% paraformaldehyde for 20 minutes at room temperature. The cells were stained with Hoechst 33342 (1 μg/mL) for 10 minutes at room temperature. After PBS washing, the cells were mounted on a glass slide with Fluoroshield™ mounting medium and imaged using the Zeiss LSM780 (Zeiss, Germany) fluorescence confocal microscope. Untreated cells were used as endogenous fluorescence controls. Two diode lasers were utilized for one-photon imaging, one at 405 nm, to excite the Hoechst 33342, with the emitted light collected in the blue region. Meanwhile, the molecules **DPP2T** and **DPP2TBr** were excited at 564 nm, and their emitted light was collected in the red region. For two-photon imaging, a Ti:Sapphire laser (800 nm, 80 MHz) was employed to excite **DPP2T** and **DPP2TBr**, and the emitted light was collected in the corresponding red region (550-650 nm).

3 RESULTS AND DISCUSSIONS

3.1 Linear photophysical properties determination

The one-photon absorption (black lines) and fluorescence emission (blue lines) spectra of the dyes dissolved in chloroform are shown in **Figure 2**.

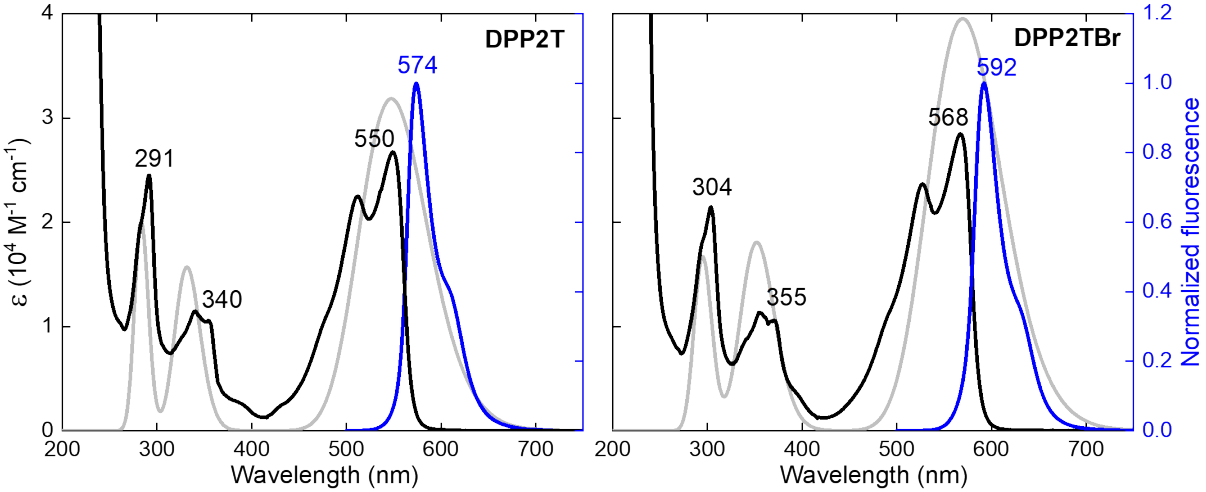

Figure 2 - One-photon absorption (black lines) and fluorescence emission (blue lines) spectrum of the dithienyl-diketopyrrolopyrrole derivatives. The gray lines are the computed one-photon absorption spectra obtained based on the results provided by TD-PCM-B3LYP calculations.

As can be seen in **Figure 2**, the dyes exhibit three electronic bands in the near-UV and visible region, which are all ascribed to 1PA allowed transitions of $\pi - \pi^*$ nature originating from a local excitation transition[40,41] (see **Figure 3**). The lowest energy electronic band is located at *c.a.* $560\ nm$ ($2.2\ eV$) with a molar absorptivity on the order of $2.8 \cdot 10^4\ M^{-1}cm^{-1}$, displaying well-defined vibrational progressions separated by approximately $170\ meV$, consistent with the C-C, C=C, and C-N-C stretch vibrational mode[42,43]. On the other hand, the second and third electronic bands occur around $348\ nm$ and $298\ nm$ ($3.56\ eV$ and $4.16\ eV$, respectively), with molar absorptivities of approximately 1.1 and $2.3 \cdot 10^4\ M^{-1}cm^{-1}$, respectively. The substitution of hydrogen atoms with bromine in **DPP2TBr** resulted in a bathochromic shift of approximately $0.14\ eV$ for all electronic transitions and an increase in the 1PA intensity. This is associated with the increased delocalization of π-electrons provided by the bromine atom (see **Figure 3**), resulting in higher molecular polarizability[44].

The computed 1PA spectra (gray lines in **Figure 2**) for **DPP2T** and **DPP2TBr** corroborated the experimental ones and indicate that these compounds have three electronic bands along the UV-Vis spectral region. The lower energy band is described by only a single electronic transition, while the two highest energy bands should be ascribed to the combination of some electronic transitions (see **Table SI2**). Another noteworthy result from the QCCs is the presence of two transitions at approximately $400\ nm$ with a null oscillator strength, indicating that these states are optically "dark" for 1PA. The theoretical results showed relatively small differences compared to the experimental values, with the maximum difference in absorption energy being less than

299 $0.13\ eV$. However, it was observed that the theoretical results overestimated the intensity
300 of the electronic transitions, and consequently the amplitude of the absorption bands
301 observed, which is a common characteristic of TD-DFT calculations[44–46].

302 The fluorescence emission spectra (**Figure 2** blue lines) of the dithienyl-
303 diketopyrrolopyrrole derivatives were obtained by exciting them at $500\ nm$. The
304 fluorescence constitutes the visible region in a range from $550\ nm$ to $700\ nm$, showing
305 partway resolved vibronic progressions. Comparing to **DPP2T** the emission peak of
306 **DPP2TBr** is redshift by about $0.07\ eV$. Analyzing the difference between the
307 fluorescence emission peak and the lowest energy transition, an average Stokes shift ($\Delta\bar{\nu}$,
308 in cm^{-1}) value of *ca.* $737\ cm^{-1}$, relatively small, was noted. This suggests that the
309 molecules have a similar electronic structure in both the excited and ground states[47], a
310 behavior that becomes more evident when analyzing the molecular orbitals (MOs) (see
311 **Figure 3**).

312 **Table 1** summarizes other compounds' properties, including fluorescence
313 quantum yield (ϕ_{fl}) and fluorescence lifetime (τ_{fl}). The analysis of emissive properties
314 revealed distinct behaviors in their photophysical characteristics. The τ_{fl} (in chloroform)
315 were determined as 6.0 ns for **DPP2T** and 5.7 ns for **DPP2TBr**, indicating comparable
316 time scales for relaxation processes in both molecules. Despite the subtle difference in
317 lifetime, these molecules exhibited more distinct ϕ_{fl} values, with 73% and 56% for
318 **DPP2T** and **DPP2TBr**, respectively. The reduction in ϕ_{fl} for **DPP2TBr** suggests a less
319 efficient conversion of absorbed photons into emitted photons, as evidenced by non-
320 radiative decay rate (k_{nr}, in s^{-1}) values (see **Table 1**). This 1.3 times decrease in ϕ_{fl} can
321 be attributed to the presence of the heavy bromine atom; it is known that this atom has
322 fluorescence quenching character[48–50]. Finally, it should be noted that these values fall
323 within the range reported for other diketopyrrolopyrrole derivatives[17,43,51–55].

324

325 **Table 1** - Photophysical properties of the dithienyl-diketopyrrolopyrrole derivatives, including Stokes shift
326 ($\Delta\bar{\nu}$), fluorescence lifetime (τ_{fl}), fluorescence quantum yield (φ_{fl}), radiative and non-radiative decay rates
327 (k_r and k_{nr}, respectively), and the difference between the permanent dipole moment, experimental and
328 theoretical, of the first excited and ground state ($|\Delta\vec{\mu}_{01}|$ and $|\Delta\vec{\mu}_{01}^{Th}|$, respectively).

	$\Delta\bar{\nu}\ (cm^{-1})$	$\tau_{\mathrm{fl}}\ (ns)$	φ_{fl} (%)		k_r ($\times 10^9 s^{-1}$)	k_{nr} ($\times 10^9 s^{-1}$)	$\lvert\Delta\vec{\mu}_{01}\rvert\ (D)$	$\lvert\Delta\vec{\mu}_{01}^{Th}\rvert$ ($\times\ 10^{-3}\ D$)*
DPP2T	760	6.0 ± 0.6	73 ± 7**	76 ± 7***	0.12	0.05	0.5 ± 0.2	0.9
DPP2TBr	714	5.7 ± 0.6	56 ± 6**	45 ± 5***	0.10	0.08	0.04 ± 0.01	9.7

329 * Difference in permanent dipole moment between the first excited state and the ground state obtained via
330 TD-PCM-B3LYP calculations.
331 ** Dissolved in Chloroform

*** Dissolved in DMSO

Figure 3 shows the MOs for the transitions with the highest oscillator strengths and, consequently, those that best represent the three electronic absorption bands. It can be observed that all three excitations are predominantly described by a $\pi \rightarrow \pi^*$ local excitation transition, with only a rearrangement of charge distribution in their excitations and a symmetric charge distribution. This symmetric configuration is a typical behavior of compounds with a centrosymmetric nature. Indeed, Polak *et al.*[16] and Zadeh *et al.*[17] attribute the symmetry of **DPP2Ts** to the C_{2h} point group, reinforcing the observation. Another point to be noted is the increased electronic distribution provided by the bromine atom, showing that, indeed, **DPP2TBr** has a higher polarizability compared to the Br-free molecule. This behavior is also evident in the reduction of the orbital energy gap.

To better understand the electronic distribution of the compounds, the difference between the permanent dipole moment of the first-excited and ground states ($|\Delta\vec{\mu}_{01}|$) was determined using the Lippert-Mataga equation[56,57]. For this purpose, solvatochromism measurements were carried out to obtain the Stokes shift as a function of solvent orientation polarizability (ΔF). The results of these measurements, including absorption and fluorescence emission spectra for different solvents, can be found in **Section 5** of the SI.

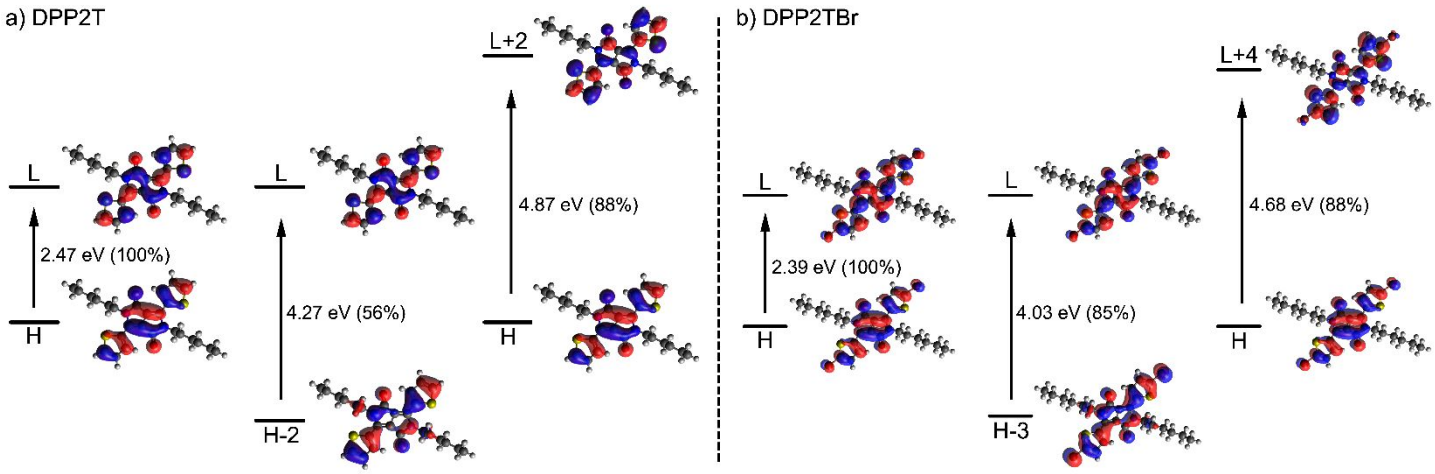

Figure 3 – Representation of molecular orbitals (H: HOMO, L: LUMO) describing transitions with the highest oscillator strengths in dithienyl-diketopyrrolopyrrole derivatives, along with the respective percentage contributions of the excitations. Results obtained from TD-PCM-B3LYP calculations.

The lowest-energy absorption and fluorescence emission bands of the molecules exhibited a subtle spectral shift concerning the ΔF (as can be seen **Figure SI4 and Figure**

SI5). This behavior was expected, given that the molecules underwent only an electronic charge redistribution upon electronic excitation, and, according to TD-DFT calculations performed by Polak[16], no conformational changes were observed in the first excited state compared to the ground one. As a result, $\Delta\bar{\nu}$ remained nearly constant concerning ΔF, indicating that the permanent dipole moment of the excited state is very similar to that of the ground one. Finally, by conducting a linear regression, it was possible to obtain the line slope ($\Delta\nu/\Delta F$, in cm^{-1}), allowing the estimation of $|\Delta\vec{\mu}_{01}|$ using the Lippert-Mataga equation[58,59].

Table 1 reveals that, within the experimental precision and considering the approximations of the Lippert-Mataga equation, the $|\Delta\vec{\mu}_{01}|$ values for **DPP2TBr** and **DPP2T** are low ($0.04\,D$ and $0.5\,D$, respectively). Additionally, TD-PCM-B3LYP calculations also indicated that the $|\Delta\vec{\mu}_{01}|$ is negligible for both compounds (see $|\Delta\vec{\mu}_{01}^{Th}|$ in **Table 1**). These results, therefore, constitute yet another strong evidence of the compounds charge symmetry nature[60–62].

3.2 Two-photon absorption determination and SOS model analyses

The 2PA cross-sections, σ^{2PA}, of the dithienyl-diketopyrrolopyrrole derivatives were determined by the open aperture tunable femtosecond Z-scan technique, spectrally resolved over a range of $790-1000\,nm$, with $10\,nm$ resolution. The obtained spectroscopic data are summarized in **Table 2**. **Figure 4** shows the 1PA (black lines) and σ^{2PA} (black circles) spectra together to facilitate the comparison. The fittings of the open-aperture z-scan curves are showed in **Figure SI3.**

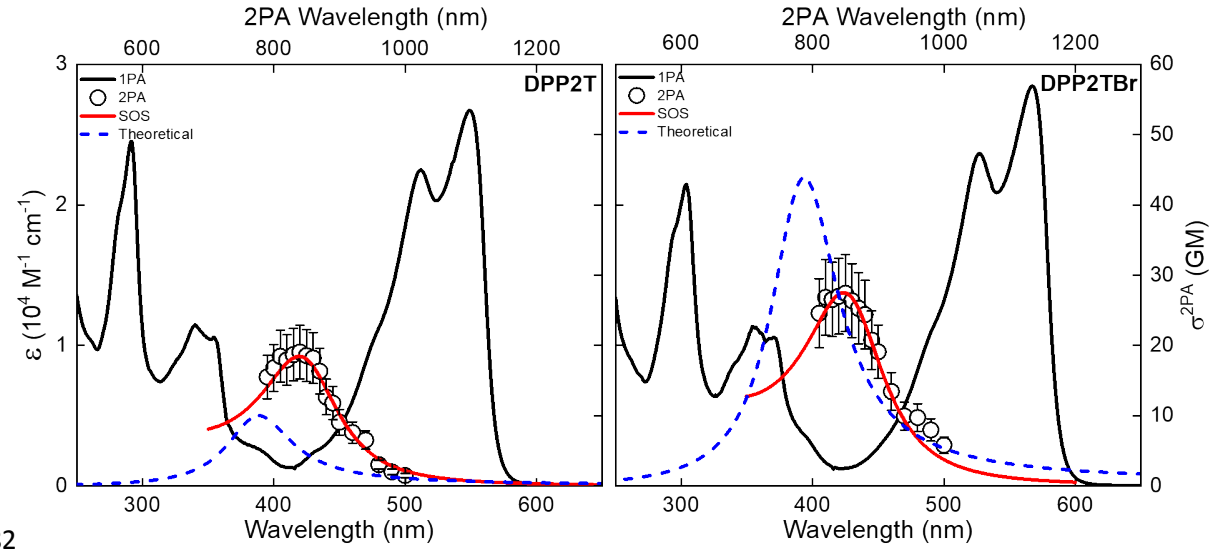

Figure 4 – One-photon absorption (black lines) spectrum and two-photon absorption cross-section spectrum (Black circles and blue dashed lines represent experimental and theoretical results, respectively.) of dithienyl-diketopyrrolopyrrole derivatives. The red line represents the fit using the SOS model.

Table 2 – Nonlinear optical properties of the investigated dithienyl-diketopyrrolopyrrole derivatives, including the experimental and theoretical 2PA wavelength at peak (λ^{2PA} and λ_{Th}^{2PA}, respectively), experimental and theoretical 2PA cross-section at peak (σ^{2PA} and σ_{Th}^{2PA}, respectively), the transition dipole moment from the ground state to the first excited one ($|\vec{\mu}_{01}|$), and the two-photon brightness ($\sigma^{2PA} \cdot \varphi_{fl}$).

Molecules	λ^{2PA} (nm)	σ^{2PA} (GM)	λ_{Th}^{2PA} $(nm)^*$	σ_{Th}^{2PA} $(GM)^*$	$\lvert\vec{\mu}_{01}\rvert$ (D)	$\lvert\vec{\mu}_{12}\rvert$ $(D)^{**}$	$\sigma^{2PA} \cdot \varphi_{fl}$ (GM)
DPP2T	840	19 ± 4	790	12	6.1 ± 0.6	4.3	14 ± 3
DPP2TBr	850	27 ± 5	800	36	6.3 ± 0.6	4.7	15 ± 3

* Nonlinear properties obtained from QRF-PCM-B3LYP calculation;
** Transition dipole moment from the first excited state to the second excited one as determined by the SOS model.

From **Figure 4**, it can be observed that the 2PA electronic band is located in the near-IR region; at 840 nm (~1.47eV) for **DPP2T**, with a value of 19 GM, and at 850 nm (~1.46 eV) for **DPP2TBr**, with a value of 27 GM. An interesting behavior to note is the decrease in the σ^{2PA} values within the lower energy band; the reason for this will become clearer shortly. Similar to what was observed for 1PA, the substitution of hydrogen atom by bromine in **DPP2TBr** led to a 1.4-fold increase in the σ^{2PA} value and a subtle bathochromic shift of approximately 0.02 eV. It is important to highlight that similar behaviors have also been reported for other diketopyrrolopyrrole derivatives[17,22,43,55,63].

In **Figure 4**, it is also possible to visualize the first 2PA allowed electronic band (dashed blue lines) obtained through QRF-PCM-B3LYP calculations. Additional data and some calculation details can be found in **Section 2** of the SI. The results revealed a two-photon transition at 790 nm (1.57 eV) and 800 nm (1.55 eV) for **DPP2T** and **DPP2TBr**, respectively. Comparing theoretical and experimental results, a difference in

energy of less than $0.15\ eV$ is observed. Regarding σ^{2PA}, the QQCs exhibited distinct behaviors for the two compounds; for **DPP2T**, the theoretical result underestimated the values of σ^{2PA} ($12\ GM$), while for **DPP2TBr**, the value was overestimated ($36\ GM$), resulting in an average error of 42%. However, it is worth highlighting that the increase of σ^{2PA} when we compare the experimental values obtained for **DPP2T** and **DPP2TBr** is correctly described by the QQCs. In summary, what should be emphasized is that both experimental and theoretical results show that 2PA occurs in a spectral region different from 1PA, and the increase in the σ^{2PA} is solely due to the greater electronic delocalization provided by the bromine atom.

These results indicate that the electronic transition performed by 2PA ($1A_g$-like → $2A_g$-like) is scarcely accessible by 1PA, *i.e.*, the $2A_g$-like state is optically "dark" for 1PA. From the TD-DFT calculations (refer to **Table SI2**), this transition ($1A_g$-like → $2A_g$-like) showed an oscillator strength of zero for 1PA, resulting in a transition by 2PA, as seen in **Figure 4**. The explanation for this behavior is associated with the centrosymmetric nature of the compounds. Due to the dipole selection rule, this causes states that are optically "dark" for 1PA to become optically "bright" for 2PA[64–66].

Figure SI2 shows the MOs involved in the first excited-state allowed by 2PA, which, in this case, corresponds to the HOMO-1 → LUMO excitation (contributions ranging by $87 - 94\%$). Unlike what was observed in **Figure 3**, electronic excitations by 2PA correspond to an intramolecular charge transfer process, now with a small involvement of the hexyl chain. Thus, in the excitation from HOMO-1 to LUMO, there is a charge displacement from the diketopyrrolopyrrole/hexyl core to the thienyl lateral moieties, with their respective ligands H or Br.

In view of improving the 2PA process interpretation, the Sum-Over-States (SOS) approach was employed, considering a three-level energy system[62,67]. The model consists of a ground state ($1A_g$-like), an intermediate excited-state allowed by 1PA ($1B_u$-like) and a final excited-state allowed by 2PA ($2A_g$-like)[67]. Such model is described by the following equation:

$$\sigma^{2PA} = \frac{2}{5}\frac{(2\pi)^4}{(chn)^2}L^4\frac{1}{\pi}\left[\frac{\nu^2}{(\nu_{01} - \nu)^2 + \Gamma_{01}^2}\frac{|\vec{\mu}_{01}|^2 \cdot |\vec{\mu}_{12}|^2 \cdot \Gamma_{02}}{(\nu_{02} - 2\nu)^2 + \Gamma_{02}^2}\right] \quad (1)$$

in this equation c, h, n, and L are light speed, Planck constant, refractive index (1.446 for the chloroform) and the Onsager local field factor, respectively. ν, ν_{0i} and Γ are laser

pulse frequency, transition frequency from the ground state to the *ith* excited state, and the Full Width at Half Maximum (FWHM) considering a Lorentzian curve, respectively. Finally, $|\vec{\mu}_{01}|^2 \cdot |\vec{\mu}_{12}|^2$ is the tree-states term. **Figure 3** (red lines) shows the 2PA spectrum fit using equation (1), while **Table 2** lists such photophysical properties. For the application of the SOS model, two parameters are necessary: the transition dipole moment from the ground state to the first excited one ($|\vec{\mu}_{01}|$, in *D*) (presented in **Section 6** of the SI) and the transition dipole moment from the first excited state to the second excited one ($|\vec{\mu}_{12}|$, in *D*), which in this case was considered as a fitting parameter[68]. Overall, the three-level model adequately describes the experimental data. A significant contribution of the coupling between the ground state and the first excited one is observed in comparison to the coupling between the first excited state and the second one, as indicated by the ratio $\frac{|\vec{\mu}_{01}|}{|\vec{\mu}_{12}|} \approx 1.4$, for the σ^{2PA}.

Fluorescence emission measurements induced by 2PA were carried out to verify if the fluorescence of dithienyl-diketopyrrolopyrrole could be triggered by pure 2PA. The samples were excited at 850 nm and 900 nm. **Figure 5** shows the fluorescence spectrum of the compounds excited at 850 nm for different laser pulse intensities. As expected, the spectra are similar to those observed by 1PA. The small inset in **Figure 5** reveals the two-photon induced nature of the fluorescence emission. The slope of the line on the log x log scale of the fluorescence intensity as a function of pulse energy is equal to 2.0, evidencing a quadratic dependence[66,69]. It would be appropriate to emphasize that, due to their high φ_{fl} and occurrence of 2PA in the infrared spectral region, which constitutes the therapeutic window[70], these compounds are promising for applications in fluorescent probes with moderate two-photon brightness ($\sigma^{2PA} \cdot \varphi_{\mathrm{fl}}$, in GM) (see **Table 2**).

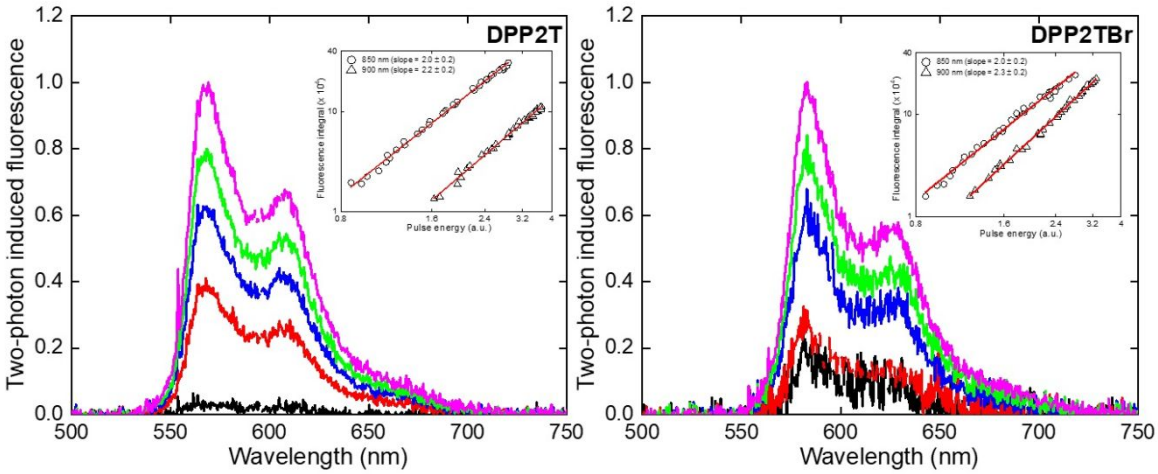

Figure 5 – Two-photon absorption induced fluorescence emission of the dithienyl-diketopyrrolopyrrole derivatives. The inset portrays the fluorescence signal versus laser pulse energy in the log x lox scale, excited at 850 nm (circles) and 900 nm (triangle). Solid lines show quadratic dependence on the 2PA fluorescence process.

3.3 Toxicity, internalization, and cell imaging.

To explore the potential of the **DPP2T** and **DPP2TBr** as fluorescent stains for cell imaging, we evaluated their biocompatibility and uptake by the HDFn cell line. The biocompatibility of **DPP2T** and **DPP2TBr** on HDFn cells showed negligible deleterious effects (low toxicity) (**Figure 6a**), later confirmed by Confocal Laser Scanning Microscopy (CLSM) images, in which the cells incubated with **DPP2T** or **DPP2TBr** showed no morphological damage (**Figure 6b**). For CLSM analyses, we used Hoechst 33342 as a reference nuclear stain, excited at 405 nm, while **DPP2T** and **DPP2TBr** were used as fluorescent stains, both excited at 564 nm. Under one-photon (**Figure 6b**) and two-photon excitations (**Figure 7),** the **DPP2T** showed robust cellular uptake and uniform intracellular distribution, exhibiting higher red fluorescence than control cells after 1 hour of incubation (**Figure 6b**). CLSM images, depicted the compound's cellular uptake and diffusion within the cytoplasmic region while revealing its inability to internalize the cell nucleus. Notably, **DPP2T** staining resisted paraformaldehyde fixation, providing versatility for multiparametric imaging. Conversely, **DPP2TBr** compound showed red fluorescence comparable to control cells, suggesting its limited capacity to internalize HDFn cells, the same behavior was observed for two-photon excitation.

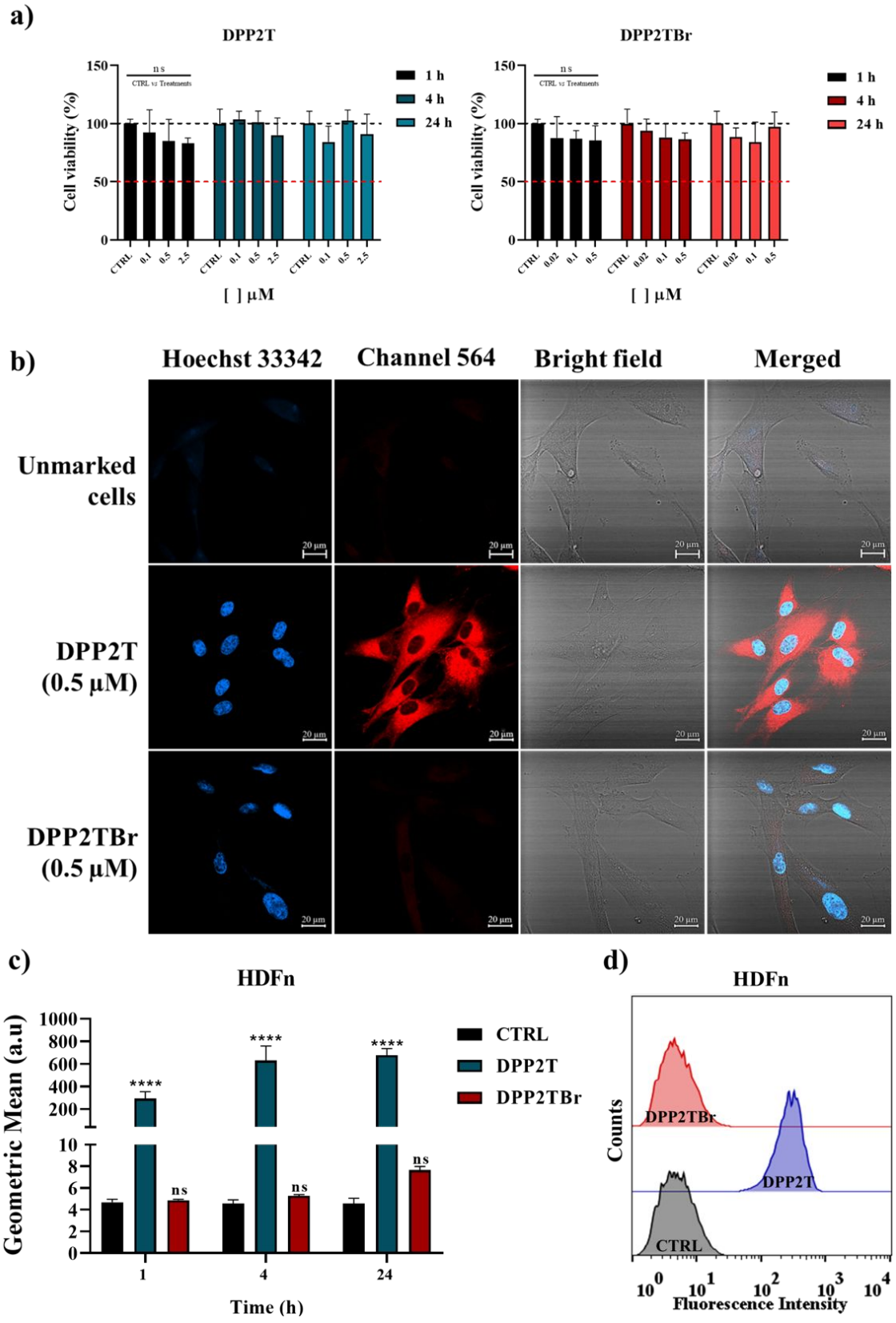

Figure 6 - *In vitro* assessment of cell viability, internalization and bioimaging capabilities of **DPP2T** and **DPP2TBr**: (a) Viability HDFn cells following incubation with **DPP2T** and **DPP2TBr** at various concentrations for 1, 4, and 24 hours. Data presented as mean ± standard deviation (n = 9). Statistical significance assessed via one-way ANOVA followed by post hoc Tukey test. P-values indicate

nonsignificant differences between CTRL and **DPP2T**, as well as between CTRL and **DPP2TBr**. (b) Representative confocal laser scanning microscopy (CLSM) images depict HDFn cells following a 1-hour incubation with **DPP2T** (0.5 μM) and **DPP2TBr** (0.5 μM), excited at 564 nm. Hoechst 33342 was utilized to stain cell nuclei (λ_{ex} = 405 nm, depicted in blue). Scale bars: 20 μm. (c) Quantification of mean fluorescence intensities (geometric mean) for HDFn cells after 1, 4, and 24 hours of incubation with DPP2T (0.5 μM) and **DPP2TBr** (0.5 μM). (d) Flow cytometric analysis of HDFn cells following a 1-hour incubation with blank solution, **DPP2T** (0.5 μM), and **DPP2TBr** (0.5 μM). Data presented as mean ± standard deviation (n = 3). Statistical significance was determined using one-way ANOVA followed by a post hoc Tukey test. ****$p < 0.0001$.

Further investigations into the internalization of these compounds across different cellular models and endocytosis mechanisms are necessary to determine whether uptake is cell-type-dependent or is governed by physicochemical factors, such as lipophilicity and solubility, stemming from structural differences arising from the hydrogen atom replacement by bromine. We quantitatively measured the intracellular uptake of HDFn cells using flow cytometry (**Figure 6c, d**), demonstrating that after 1-hour incubation with **DPP2T**, the fluorescence intensity was 62.6-fold higher than that of unstained cells. This intensity increased over time, maintaining stability for up to 24 hours, suggesting the potential application of this organic molecule in live cell monitoring. Consistent with the confocal microscopy findings, we observed no increase in fluorescence intensity for **DPP2TBr** compared to unlabeled cells. Therefore, our data underscores the **DPP2T**'s potential as a fluorescent stain for imaging HDFn cells, while **DPP2TBr** lacks this capability for this cell line. Despite the availability of numerous commercially accessible fluorescent stains, these compounds interest researchers due to their capacity for two-photon excitation—a critical feature for tracking long-term biological processes, imaging tissues and bodies with deep penetration, and minimal endogenous fluorescence background.

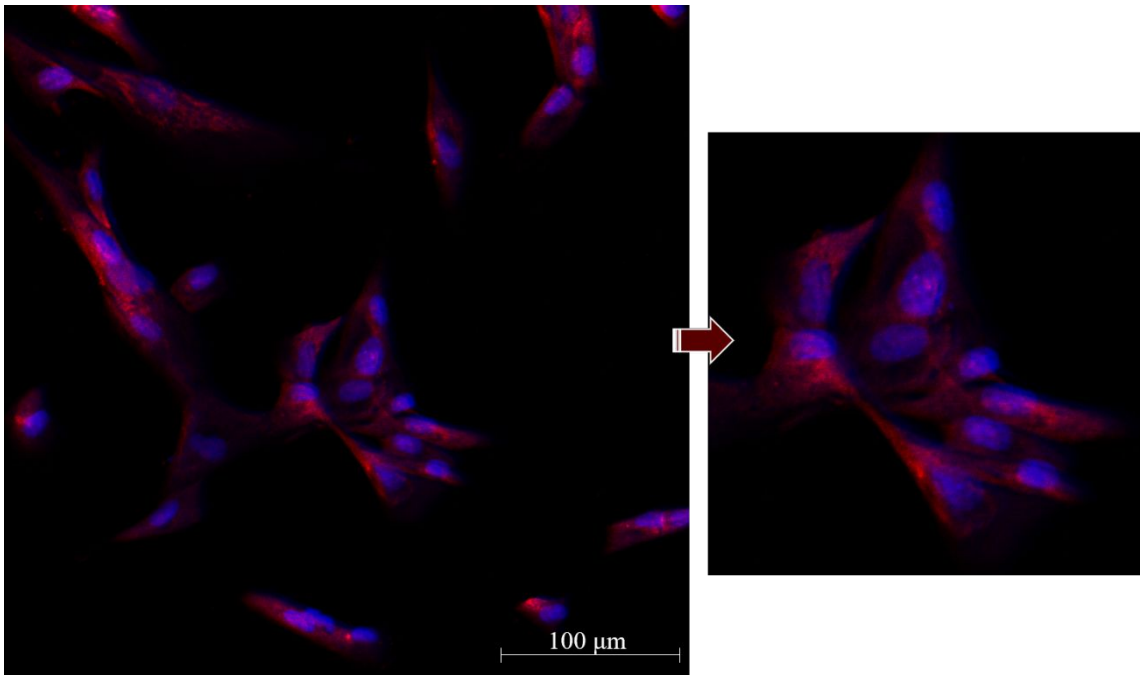

Figure 7: Representative confocal laser scanning microscopy (CLSM) images depict HDFn cells following a 1-hour incubation with **DPP2T** (0.5 µM), excited by two-photon (800 nm + Hoechst 33342).

4 CONCLUSION

We investigated the (non)linear absorption and emission properties of two dithienyl-diketopyrrolopyrrole derivatives and the influence of the bromine atom on these properties. From the 1PA spectra, three electronic bands were identified and confirmed by TD-DFT calculations, of $\pi - \pi^*$ nature. The bromine atom led to a bathochromic shift in 1PA. The compounds exhibited excellent emissive properties with fluorescence quantum yield values of 73 % and 56 % for **DPP2T** and **DPP2TBr**, respectively. In this case, the influence of the bromine atom was negative, leading to a decrease in fluorescence. Solvatochromism measurements revealed that the compounds exhibit a symmetrical charge distribution due to the centrosymmetric structure. Both compounds exhibited a 2PA band in a dark spectral region for the 1PA. The substitution of hydrogen atom with bromine in the **DPP2TBr** led to 1.4 times increase in the 2PA cross-section value. This effect was associated with a greater electronic delocalization observed in the **DPP2TBr** due to the bromine atom. Furthermore, the data underscores DPP2T's efficacy as a fluorescent stain for imaging HDFn cells, whereas DPP2TBr lacks this capability for this specific cell line. These compounds are of interest to researchers owing to their

capacity for two-photon excitation, a critical attribute enabling the tracking of long-term biological processes and imaging of tissues and organisms with deep penetration and minimal endogenous fluorescence background.

5 SUPPORT INFORMATION

Section 1 of the Supporting Information delineates the Time-Resolved Fluorescence technique, including both the experimental results and the corresponding data fittings derived from this methodology. **Section 2** details the quantum chemical calculations employed in the study. **Section 3** provides comprehensive information on Two-Photon Absorption measurements, describing the Z-Scan technique and presenting normalized transmittance data for 800 nm and 840 nm (DPP2T), as well as 820 nm and 850 nm (DPP2TBr). **Section 4** is devoted to the measurements of fluorescence induced by 2PA. **Section 5** discusses the solvatochromism measurements. **Section 6** elucidates the procedures and calculations for determining the transition dipole moment.

References

1 L. Xu, W. Lin, B. Huang, J. Zhang, X. Long, W. Zhang and Q. Zhang, *J. Mater. Chem. C*, 2021, **9**, 1520–1536.

2 L. Xu, J. Zhang, L. Yin, X. Long, W. Zhang and Q. Zhang, *J. Mater. Chem. C*, 2020, **8**, 6342–6349.

3 P. A. Shaw, E. Forsyth, F. Haseeb, S. Yang, M. Bradley and M. Klausen, *Front. Chem.*, 2022, **10**, 1–33.

4 S. Yao, H.-Y. Ahn, X. Wang, J. Fu, E. W. Van Stryland, D. J. Hagan and K. D. Belfield, *J. Org. Chem.*, 2010, **75**, 3965–3974.

5 G. S. He, L.-S. Tan, Q. Zheng and P. N. Prasad, *Chem. Rev.*, 2008, **108**, 1245–1330.

6 W. R. Zipfel, R. M. Williams and W. W. Webb, *Nat. Biotechnol.*, 2003, **21**, 1369–1377.

7 X. Wang, D. M. Nguyen, C. O. Yanez, L. Rodriguez, H.-Y. Ahn, M. V. Bondar and K. D. Belfield, *J. Am. Chem. Soc.*, 2010, **132**, 12237–12239.

8 L. M. G. Abegão, F. A. Santos, R. D. Fonseca, A. L. B. S. Barreiros, M. L. Barreiros, P. B. Alves, E. V. Costa, G. B. Souza, M. A. R. C. Alencar, C. R.

Mendonça, K. Kamada, L. De Boni and J. J. Rodrigues, *Spectrochim. Acta - Part A Mol. Biomol. Spectrosc.*, 2020, **227**, 117772.

9 A. Rebane, M. Drobizhev, N. S. Makarov, E. Beuerman, J. E. Haley, D. M. Krein, A. R. Burke, J. L. Flikkema and T. M. Cooper, *J. Phys. Chem. A*, 2011, **115**, 4255–4262.

10 M. G. Vivas, D. L. Silva, J. Malinge, M. Boujtita, R. Zaleśny, W. Bartkowiak, H. Ågren, S. Canuto, L. De Boni, E. Ishow and C. R. Mendonca, *Sci. Rep.*, 2014, **4**, 27–30.

11 M. Pieczykolan, B. Sadowski and D. T. Gryko, *Angew. Chemie*, 2020, **132**, 7598–7605.

12 G. D. Kumar, M. Banasiewicz, W. Hu, R. Hany, O. Vakuliuk, F. Nüesch, I. Deperasińska and D. T. Gryko, *ChemPhotoChem*, , DOI:10.1002/cptc.202300293.

13 D. C. Young, M. Tasior, A. D. Laurent, Ł. Dobrzycki, M. K. Cyrański, N. Tkachenko, D. Jacquemin and D. T. Gryko, *J. Mater. Chem. C*, 2020, **8**, 7708–7717.

14 Ł. G. Łukasiewicz, M. Rammo, C. Stark, M. Krzeszewski, D. Jacquemin, A. Rebane and D. T. Gryko, *ChemPhotoChem*, 2020, **4**, 508–519.

15 G. D. Kumar, M. Banasiewicz, D. Jacquemin and D. T. Gryko, *Chem. – An Asian J.*, 2021, **16**, 355–362.

16 D. W. Polak, M. T. do Casal, J. M. Toldo, X. Hu, G. Amoruso, O. Pomeranc, M. Heeney, M. Barbatti, M. N. R. Ashfold and T. A. A. Oliver, *Phys. Chem. Chem. Phys.*, 2022, **24**, 20138–20151.

17 E. H. Ghazvini Zadeh, M. V. Bondar, I. A. Mikhailov and K. D. Belfield, *J. Phys. Chem. C*, 2015, **119**, 8864–8875.

18 M. Sassi, N. Buccheri, M. Rooney, C. Botta, F. Bruni, U. Giovanella, S. Brovelli and L. Beverina, *Sci. Rep.*, 2016, **6**, 34096.

19 S. Mula, D. Hablot, K. K. Jagtap, E. Heyer and R. Ziessel, *New J. Chem.*, 2013, **37**, 303–308.

20 A. L. Neto, L. Scalon, L. Octavio de Araujo, F. Lopes de Araújo, E. R. Spada, M. R. Pereira da Cunha, J. C. Desordi, R. C. Barreto, A. G. Macedo, R. M. Faria and P. C. Rodrigues, *Mater. Chem. Phys.*, 2021, **262**, 124271.

21 X. Zou, S. Cui, J. Li, X. Wei and M. Zheng, *Front. Chem.*, , DOI:10.3389/fchem.2021.671294.

22 C. Yang, M. Zheng, Y. Li, B. Zhang, J. Li, L. Bu, W. Liu, M. Sun, H. Zhang, Y. Tao, S. Xue and W. Yang, *J. Mater. Chem. A*, 2013, **1**, 5172–5178.

23 Z. Yang, W. Xu, J. Wang, L. Liu, Y. Chu, Y. Wang, Y. Hu, T. Yi and J. Hua, *J. Mater. Chem. C*, 2020, **8**, 8183–8190.

24 M. Pieczykolan, B. Sadowski and D. T. Gryko, *Angew. Chemie Int. Ed.*, 2020, **59**, 7528–7535.

25 H. Ftouni, F. Bolze, H. de Rocquigny and J.-F. Nicoud, *Bioconjug. Chem.*, 2013, **24**, 942–950.

26 L. Scalon, A. Leithold Neto, L. O. Araujo, S. Zaioncz, J. B. Floriano, A. G. Macedo, C. M. Araujo, C. F. N. Marchiori and P. C. Rodrigues, *ACS Appl. Polym. Mater.*, 2021, **3**, 4223–4233.

27 C. Würth, M. Grabolle, J. Pauli, M. Spieles and U. Resch-Genger, *Nat. Protoc.*, 2013, **8**, 1535–1550.

28 P. C. Beaumont, D. G. Johnson and B. J. Parsons, *J. Chem. Soc. Faraday Trans.*, 1998, **94**, 195–199.

29 L. H. Zucolotto Cocca, J. V. P. Valverde, J. le Bescont, C. Breton-Patient, S. Piguel, D. L. Silva, C. R. Mendonca and L. De Boni, *J. Mol. Struct.*, 2024, **1300**, 137221.

30 M. J. Frisch, G. W. Trucks, H. B. Schlegel, G. E. Scuseria, M. A. Robb, J. R. Cheeseman, G. Scalmani, V. Barone, B. Mennucci, G. A. Petersson, H. Nakatsuji, M. Caricato, X. Li, H. P. Hratchian, A. F. Izmaylov, J. Bloino, G. Zheng, J. L. Sonnenberg, M. Hada, M. Ehara, K. Toyota, R. Fukuda, J. Hasegawa, M. Ishida, T. Nakajima, Y. Honda, O. Kitao, H. Nakai, T. Vreven, J. A. Montgomery, J. E. Peralta, F. Ogliaro, M. Bearpark, J. J. Heyd, E. Brothers, K. N. Kudin, V. N. Staroverov, R. Kobayashi, J. Normand, K. Raghavachari, A. Rendell, J. C. Burant, S. S. Iyengar, J. Tomasi, M. Cossi, N. Rega, J. M. Millam, M. Klene, J. E. Knox, J. B. Cross, V. Bakken, C. Adamo, J. Jaramillo, R. Gomperts, R. E. Stratmann, O. Yazyev, A. J. Austin, R. Cammi, C. Pomelli, J. W. Ochterski, R. L. Martin, K. Morokuma, V. G. Zakrzewski, G. A. Voth, P. Salvador, J. J. Dannenberg, S. Dapprich, A. D. Daniels, Farkas, J. B. Foresman, J. V Ortiz, J. Cioslowski and D. J. Fox, *Gaussian 09, Revis. B.01, Gaussian, Inc., Wallingford CT*, 2009, 1–20.

31 P. Sałek, O. Vahtras, J. Guo, Y. Luo, T. Helgaker and H. Ågren, *Chem. Phys. Lett.*, 2003, **374**, 446–452.

32 K. Aidas, C. Angeli, K. L. Bak, V. Bakken, R. Bast, L. Boman, O. Christiansen, R. Cimiraglia, S. Coriani, P. Dahle, E. K. Dalskov, U. Ekström, T. Enevoldsen, J. J. Eriksen, P. Ettenhuber, B. Fernández, L. Ferrighi, H. Fliegl, L. Frediani, K. Hald, A. Halkier, C. Hättig, H. Heiberg, T. Helgaker, A. C. Hennum, H. Hettema, E. Hjertenaes, S. Høst, I.-M. Høyvik, M. F. Iozzi, B. Jansík, H. J. A. Jensen, D. Jonsson, P. Jørgensen, J. Kauczor, S. Kirpekar, T. Kjaergaard, W. Klopper, S. Knecht, R. Kobayashi, H. Koch, J. Kongsted, A. Krapp, K. Kristensen, A. Ligabue, O. B. Lutnaes, J. I. Melo, K. V. Mikkelsen, R. H. Myhre, C. Neiss, C. B. Nielsen, P. Norman, J. Olsen, J. M. H. Olsen, A. Osted, M. J. Packer, F. Pawlowski, T. B. Pedersen, P. F. Provasi, S. Reine, Z. Rinkevicius, T. A. Ruden, K. Ruud, V. V. Rybkin, P. Sałek, C. C. M. Samson, A. S. de Merás, T. Saue, S. P. A. Sauer, B. Schimmelpfennig, K. Sneskov, A. H. Steindal, K. O. Sylvester-Hvid, P. R. Taylor, A. M. Teale, E. I. Tellgren, D. P. Tew, A. J. Thorvaldsen, L. Thøgersen, O. Vahtras, M. A. Watson, D. J. D. Wilson, M. Ziolkowski and H. Ågren, *Wiley Interdiscip. Rev. Comput. Mol. Sci.*, 2014, **4**, 269–284.

33 A. D. Becke, *J. Chem. Phys.*, 1993, **98**, 5648–5652.

34 D. E. Woon and T. H. Dunning, *J. Chem. Phys.*, 1995, **103**, 4572–4585.

35 T. H. Dunning, *J. Chem. Phys.*, 1989, **90**, 1007–1023.

36 E. Cancès, B. Mennucci and J. Tomasi, *J. Chem. Phys.*, 1997, **107**, 3032–3041.

37 J. Tomasi, B. Mennucci and E. Cancès, *J. Mol. Struct. THEOCHEM*, 1999, **464**, 211–226.

38 L. Frediani, Z. Rinkevicius and H. Ågren, *J. Chem. Phys.*, , DOI:10.1063/1.1944727.

39 D. S. Corrêa, L. De Boni, L. Misoguti, I. Cohanoschi, F. E. Hernandez and C. R. Mendonça, *Opt. Commun.*, 2007, **277**, 440–445.

40 H. Nitta and I. Kawata, *Chem. Phys.*, 2012, **405**, 93–99.

41 L. O. de Araujo, A. L. Neto, L. Scalon, P. C. Rodrigues, J. B. Floriano and R. C. Barreto, *Dye. Pigment.*, , DOI:10.1016/j.dyepig.2021.109140.

42 Peter J. Larkin, *Infrared and Raman Spectroscopy*, Elsevier, 2018.

43 M. Grzybowski, E. Glodkowska-Mrowka, V. Hugues, W. Brutkowski, M. Blanchard-Desce and D. T. Gryko, *Chem. - A Eur. J.*, 2015, **21**, 9101–9110.

44 A. Masunov and S. Tretiak, *J. Phys. Chem. B*, 2004, **108**, 899–907.

45 E. A. Perpète, F. Maurel and D. Jacquemin, *J. Phys. Chem. A*, 2007, **111**, 5528–5535.

46 P. N. Day, K. A. Nguyen and R. Pachter, *J. Phys. Chem. B*, 2005, **109**, 1803–1814.

47 H. Bürckstümmer, A. Weissenstein, D. Bialas and F. Würthner, *J. Org. Chem.*, 2011, **76**, 2426–2432.

48 Q. Ma, X. Sun, W. Wang, D. Yang, C. Yang, Q. Shen and J. Shao, *Chinese Chem. Lett.*, 2022, **33**, 1681–1692.

49 P. Xue, P. Wang, P. Chen, B. Yao, P. Gong, J. Sun, Z. Zhang and R. Lu, *Chem. Sci.*, 2017, **8**, 6060–6065.

50 P. Xu, Q. Qiu, X. Ye, M. Wei, W. Xi, H. Feng and Z. Qian, *Chem. Commun.*, 2019, **55**, 14938–14941.

51 C. E. Miller, M. R. Wasielewski and G. C. Schatz, *J. Phys. Chem. C*, 2017, **121**, 10345–10350.

52 C. M. Mauck, P. E. Hartnett, Y.-L. Wu, C. E. Miller, T. J. Marks and M. R. Wasielewski, *Chem. Mater.*, 2017, **29**, 6810–6817.

53 S. Pang, M. Más-Montoya, M. Xiao, C. Duan, Z. Wang, X. Liu, R. A. J. Janssen, G. Yu, F. Huang and Y. Cao, *Chem. – A Eur. J.*, 2019, **25**, 564–572.

54 M. A. Auwalu and S. Cheng, *Chemosensors*, 2021, **9**, 44.

55 O. Vakuliuk, A. Purc, G. Clermont, M. Blanchard-Desce and D. T. Gryko, *ChemPhotoChem*, 2017, **1**, 243–252.

56 N. Mataga, Y. Kaifu and M. Koizumi, *Bull. Chem. Soc. Jpn.*, 1956, **29**, 465–470.

57 E. Lippert, *Zeitschrift für Elektrochemie, Berichte der Bunsengesellschaft für Phys. Chemie*, 1957, **61**, 962–975.

58 A. G. Pelosi, L. H. Zucolotto Cocca, L. M. G. Abegão, L. F. Sciuti, S. Piguel, L. De Boni and C. R. Mendonça, *Dye. Pigment.*, 2022, **198**, 109972.

59 A. G. Pelosi, L. H. Zucolotto Cocca, S. Piguel, L. De Boni and C. R. Mendonça, *J. Mol. Liq.*, , DOI:10.1016/j.molliq.2022.119186.

60 A. Purc, K. Sobczyk, Y. Sakagami, A. Ando, K. Kamada and D. T. Gryko, *J. Mater. Chem. C*, 2015, **3**, 742–749.

61 T. He, Y. Gao, S. Sreejith, X. Tian, L. Liu, Y. Wang, H. Joshi, S. Z. F. Phua, S. Yao, X. Lin, Y. Zhao, A. C. Grimsdale and H. Sun, *Adv. Opt. Mater.*, 2016, **4**, 746–755.

62 M. G. Vivas, L. De Boni and C. R. Mendonça, in *Molecular and Laser Spectroscopy*, Elsevier, 2018, pp. 165–191.

63 E. Q. Guo, P. H. Ren, Y. L. Zhang, H. C. Zhang and W. J. Yang, *Chem. Commun.*, 2009, 5859–5861.

64 K. D. Bonin and T. J. McIlrath, *J. Opt. Soc. Am. B*, 1984, **1**, 52.

65 L. M. G. Abegão, R. D. Fonseca, T. N. Ramos, F. Mahuteau-Betzer, S. Piguel, J. R. Joatan, C. R. Mendonça, S. Canuto, D. L. Silva and L. De Boni, *J. Phys. Chem. C*, 2018, **122**, 10526–10534.

66 L. H. Zucolotto Cocca, L. M. G. Abegão, L. F. Sciuti, R. Vabre, J. de Paula Siqueira, K. Kamada, C. R. Mendonca, S. Piguel and L. De Boni, *J. Phys. Chem. C*, 2020, **124**, 12617–12627.

67 L. M. G. Abegão, L. H. Z. Cocca, J.-C. Mulatier, D. Pitrat, C. Andraud, L. Misoguti, C. R. Mendonça, M. G. Vivas and L. De Boni, *Phys. Chem. Chem. Phys.*, 2021, **23**, 18602–18609.

68 L. H. Zucolotto Cocca, A. G. Pelosi, L. M. G. Abegão, R. de Q. Garcia, J.-C. Mulatier, D. Pitrat, C. Barsu, C. Andraud, C. R. Mendonça, M. G. Vivas and L. De Boni, *Phys. Chem. Chem. Phys.*, 2023, **25**, 5021–5028.

69 D. S. Correa, L. De Boni, B. Nowacki, I. Grova, B. D. Fontes, P. C. Rodrigues, J. R. Tozoni, L. Akcelrud and C. R. Mendonça, *J. Polym. Sci. Part B Polym. Phys.*, 2012, **50**, 148–153.

70 F. Bolze, S. Jenni, A. Sour and V. Heitz, *Chem. Commun.*, 2017, **53**, 12857–12877.

June, 07h, 2024

Subject: Data Availability Statement

The authors confirm that the data supporting the conclusions of this study are available in the article and its supplementary materials.

Sincerely yours,

Prof. Dr. Leandro H. Zucolotto Cocca
Photonics Group, Goiás Federal University